Supporting Information

The performance and stability of oxygen reduction reaction on Pt-M (M=Pd, Ag and Au) nanorods: An experimental and computational study

Yu-Ting Liang,[a] Syuan-Pei Lin,[b] Chen-Wei Liu,[c] Shu-Ru Chung,[d]

Tsan-Yao Chen,[e] Jeng-Han Wang,[b],* and Kuan-Wen Wang [a],*

[a] Institute of Materials Science and Engineering, National Central University, Taoyuan 320, Taiwan

[b] Department of Chemistry, National Taiwan Normal University, Taipei 116, Taiwan

[c] Green Energy and Environment Research Laboratories, Industrial Technology Research Institute, Hsinchu 310, Taiwan

[d] Graduate Institute of Materials Science and Green Energy Engineering, National Formosa University, Yunlin 632, Taiwan

[e] Department of Engineering and System Science, National Tsing-Hua University, Hsinchu 300, Taiwan

*To whom correspondence should be addressed,

* Jeng-Han Wang, Electronic mail: jenghan@ntnu.edu.tw

* Kuan-Wen Wang, Electronic mail: kuanwen.wang@gmail.com

1. Experimental Section

1.1 Preparation of catalysts

Carbon-supported PtM (M=Au, Ag and Pd) NRs with metal loading about 50 wt% and Pt/M ratio of 3/1 were prepared by formic acid method (FAM). 1.5 mM of H_2PtCl_6 (Alfa Aesar) was mixed with 0.05 g of carbon black (Vulcan XC-72R), and then reduced by 10 ml of formic acid (98%) at room temperature for 216 h and 0.5 mM of $HAuCl_4$, $Pd(NO_3)_2$ or $AgNO_3$ (all from Aldrich) was added and reduced by formic acid for another 48 h. The as-prepared NRs were washed, dried and named as PtM. Besides, Pt/C (46 wt%, TKK, Tanaka Kikinzoku Kogyo) catalyst was used for the comparison.

1.2 Characterization of catalysts

The X-ray photoelectron spectroscopy (XPS) (Thermo VG Scientific Sigma Probe) using a monochromatic X-ray source (Al K_α) at a voltage of 20 kV and a current of 30 mA was executed to identify the surface chemical states of the catalysts. The morphologies of the catalysts were analyzed by high resolution transmission electron microscopy (HR-TEM) operated at a voltage of 200 kV.

In each TPR analysis, a sample of approximately 20 mg was inserted into a U-shape quartz tube and pre-oxidized in air at room temperature (300 K) for 1 h. Subsequently, the pre-oxidized catalysts (alloy or reference samples) were reduced by a flow of 20% H_2 in N_2 at a flow rate of 30 mL min^{-1} upon increasing the temperature

from 118 to 473 K at a heating rate of 7 K min^{-1}. Once the reduction process was started, the rate of hydrogen consumption presented in the TPR profile was measured automatically by a thermal conductivity detector (TCD). Moreover, silica gel and molecular sieve absorbents were utilized for the purpose of water removal before the flowing gas reached the detector.

The exact metal loadings of catalysts were determined by thermal gravimetric analysis (TGA, Perkin Elmer TGA-7). Initially, a small amount of catalysts was placed into a Pt basket and heated in a temperature range from 323 to 1073 K with a heating rate of 10 K min^{-1} under air atmosphere. The exact atomic compositions of the catalysts were examined by inductively coupled plasma-atomic emission spectrometer (ICP-AES, Jarrell-Ash, ICAP 9000).

The typical XAS spectra of various catalysts were obtained in fluorescence mode at the BL01C1 and 17C beamlines at the National Synchrotron Radiation Research Center (NSRRC), Taiwan. A Si monochromator was employed to adequately select the energy with a resolution $\Delta E/E$ better than 10^{-4} at the Pt L_{II} -edge (13273 eV), Pt L_{III} -edge (11563 eV), Ag K-edge (25514), and Pd K-edge (24350 eV). All catalysts were dispersed uniformly on the tape and prepared as thin pellets with an appropriate absorption thickness ($\mu x=1.0$, where μ is the X-ray attenuation coefficient at the absorption edge and x is the thickness of the sample) to attain a proper edge jump step

at the absorption edge region. In order to acquire acceptable quality spectra with good quality, each measurement was repeated at least twice and averaged for successive comparison. For the EXAFS analysis, the backgrounds of the pre-edge and the post-edge were subtracted and normalized with respect to the edge jump step from the XAS spectra. The normalized spectra were transformed from energy to k-space and further weighted by k^3 to distinguish the contributions of back scattering interferences from different coordination shells. Normally, the backscattered amplitude and phase shift functions for specific atom pairs were theoretically estimated by means of utilizing the FEFF7 code.

The electrochemical measurements were conducted by a CHI611C potentiostat and a classical electrochemical cell with a three-electrode configuration as reported previously.[1] All potentials in this study were referred to normal hydrogen electrode (NHE). Oxygen reduction current was gauged by linear sweep voltammetry (LSV) with a scan rate of 5 mV s^{-1} and a rotational rate of 1600 rpm. The accelerated durability tests (ADT) were obtained in the potential range of 0.6 to 1.2 V with the applied scan rate of 50 mV s^{-1} under O_2 atmosphere for 1000 cycles. The cyclic voltammograms (CV) were obtained from 0.0 to 1.2 V with scan rate of 20 mV s^{-1} under N_2 atmosphere. The electrochemical surface area (ECSA) was calculated by measuring the areas of H desorption between 0.05 and 0.4 V after the deduction of the

double-layer region by use of following equation:

where Q_H depicts the charge for H-desorption (mC cm^{-2}) and 0.21 is the charge

$$\mathrm{ECSA} = \frac{Q_H}{0.21} \quad (1)$$

required to oxidize a monolayer of H_2 on clean Pt.

The kinetic current density (I_k) was calculated based on the equation below:

$$\mathrm{I}_k = \frac{I_d I}{I_d - I} \quad (2)$$

where I, I_k and I_d are the experimentally measured, mass transport free kinetic and diffusion-limited current densities, respectively. For each electrocatalyst, the MA and SA were obtained when I_k was normalized to the Pt loading and ECSA, respectively.

1.3 Computational methods

DFT calculation with a 3D periodic boundary condition implemented in Vienna Ab initio Simulation Package (VASP)[2] was employed in the present study. The exchange-correlation function employed generalized gradient approximation[3] at the GGA-PW91 level.[4] The basis plane waves liminted to maximum of 600-eV cutoff energy were utilized to expand valence electrons. The pseudopotentials with projector-augmented wave method (PAW)[5] were applied to treat ion-core interactions. The Brillouin-Zone (BZ) integration was sampled at 0.05 × 2 (1/Å) interval by Monkhorst-Pack scheme[6] in the reciprocal space. All the modeled slabs and stable

adsorptions were optimized by quasi-Newton method with an energetic convergence of 1×10^{-4} eV and a gradient convergence of 1×10^{-2} eV.

The alloyed electrodes were modeled on the basis of Pt(111) surface by replacing surface or subsurface Pt atoms with dopants (M = Pd, Ag and Au). The (111) surface was constructed by a five-layer slab with an equivalent five-layer vacuum space to limit the artificial interaction between the distinct slabs. Each slab has a 4 × 4 surface unit and the top three layers were free to relax while the bottom two layers were fixed at the computed lattice constants to simulate the semi-infinite bulk crystal. Two commonly studied alloys,[7] in which dopants in locate in the subsurface and on the surface (donated as M@Pt and Pt@M, respectively), were investigated in the present calculation. M@Pt is constructed by replacing the first subsurface Pt with M layer, while Pt@M is made by uniformly exchanging four surface Pt with subsurface M atoms from M@Pt.

All the adsorption sites on the surfaces of modeled alloys, M@Pt and Pt@M, are plotted in Figure S6. Four possible sites, top (T), bridge (B), hcp (H) and fcc(F), were examined on M@Pt (or clean Pt). Six possible sites, Pt top (T_{Pt}), M top (T_M), bridge Pt-M (B), hcp on subsurface Pt (H_{Pt}), hcp on subsurface M (H_M) and fcc sites were examined on Pt@M. The computed E_{ads}(O*) and E_{ads}(OH*) on those sites, listed in Table S3, found that O* preferentially adsorbed on fcc sites while OH*

preferentially adsorbed on bridge sites on all the modeled surfaces. These most stable adsorptions, agreeing with previous studies,[7] were utilized in examining the oxophilicity and ORR activity of pure Pt and its alloys in the comparison with electrochemical experiment (Figure 3).

Reference

[1] a)H. S. Chen, Y. T. Liang, T. Y. Chen, Y. C. Tseng, C. W. Liu, S. R. Chung, C. T. Hsieh, C. E. Lee and K. W. Wang, *Chem. Commun.* **2014**, *50*, 11165. b) Y. C. Tseng, H. S. Chen, C. W. Liu, T. H. Yeh and K.W. Wang, *J. Mater. Chem. A* **2014**, *2*, 4270.

[2] a) G. Kresse and J. Hafner, *Phys. Rev. B* **1993**, *47*, 558. b) G. Kresse and J. Hafner, *Phys. Rev. B* **1994**, *49*, 1425. c) G. Kresse and J. Furthmüller, *Phys. Rev. B* **1996**, *54*, 11169.

[3] D. M. Cleperley and B. J. Alder, *Phys. Rev. Lett.* **1980**, *45*, 566.

[4] J. P. Perdew and Y. Yang, *Phys. Rev. B* **1992**, *45*, 244.

[5] a) P. E. Blöchl, *Phys. Rev. B* **1994**, *50*, 17953. b) G. Kresse, D. Joubert, *Phys. Rev. B* **1999**, *59*, 1758.

[6] H. J. Monkhorst and J. D. Pack, *Phys. Rev. B* **1976**, *13*, 5188.

[7] a) J. Greeley and M. Mavrikakis, *Nature Mater.* **2004**, *3*, 810; b) D. Cheng, X. Qiu and H. Yu, *Phys. Chem. Chem. Phys.* **2014**, *16*, 20377; c) X. Zhang, S. Yu, W. Zheng and P. Liu, *Phys. Chem. Chem. Phys.* **2014**, *16*, 16615; d) Z. Duan and G. Wang, *Phys. Chem. Chem. Phys.* **2011**, *13*, 20178.

Table S1 The data analyses of TGA, ICP, XRD patterns, MA_{085}, and decay rates of PtM NRs and Pt/C.

Samples	Pt metal loading	Pt:M (at %)	(111)+(220) /(200)	MA_{085} (mA/mg $_{Pt}$)		Decay (%)
				1^{st}	1000^{th}	
PtAu	35.0	72:28	2.68	117.2	89.4	23.7
PtAg	37.1	75:25	2.69	103.1	93.9	8.9
PtPd	35.1	71:29	2.66	102.7	67.3	34.4
Pt/C	46.0	100:0	2.60	90.0	17.1	71.1

Table S2 The EXAFS fitting results of PtAg and PtPd NRs.

Sample	shell	N	R[Å]	σ^2(x10^{-3}) [Å ^{2}]	ΔE_0 [eV]	R factor
PtAg	Pt-Pt	8.23	2.76	5.25	8.11	0.001
	Pt-Ag	0.31	2.56			
	Ag-Ag	4.43	2.84	5.25	3.94	
	Ag-Pt	1.98	2.56			
PtPd	Pt-O	0.59	1.97	5.69	7.01	0.001
	Pt-Pt	7.57	2.75			
	Pd-O	1.17	1.99			
	Pd-Pt	0.77	2.73	2.09	-1.88	0.004
	Pd-Pd	2.00	2.74			

Table S3 (a) E_{ads}(O*) and E_{ads}(OH*), in eV, on all possible sites of Pt(111) and Pt@M. (b) E_{ads}(O*) and E_{ads}(OH*) on all the possible sites of Pt(111) and M@Pt. The most stable adsorptions with the highest E_{ads} are in bold.

	E_{ads}(O*)				E_{ads}(OH*)			
	Pt(111)	Pt@Au	Pt@Ag	Pt@Pd	Pt(111)	Pt@Au	Pt@Ag	Pt@Pd
T	-3.19	-2.93	-3.55	-3.17	-2.39	-2.19	-2.09	-2.35
B	-3.89	-3.99	-4.04	-3.93	**-2.46**	**-2.51**	**-2.21**	**-2.42**
H	-4.42	-4.45	-4.41	-4.28	-2.30	-2.09	-1.95	-2.00
F	**-4.52**	**-4.57**	**-4.51**	**-4.51**	-2.33	-2.25	-2.01	-2.23

	E_{ads}(O*)				E_{ads}(OH*)			
	Pt(111)	Au@Pt	Ag@Pt	Pd@Pt	Pt(111)	Au@Pt	Ag@Pt	Pd@Pt
T_{Pt}	-3.19	-3.10	-2.83	-3.42	-2.39	-2.12	-2.42	-2.49
T_M	--	-1.52	-0.89	-2.05	--	-1.51	-1.40	-2.08
B	-3.89	-3.16	-3.87	-3.93	**-2.46**	**-2.14**	**-2.43**	**-2.54**
H_{Pt}	-4.42	-3.46	-3.86	-4.22	-2.30	-1.72	-2.04	-2.26
H_M	--	-3.70	-4.05	-4.29	--	-1.86	-2.17	-2.20
F	**-4.52**	**-4.05**	**-4.21**	**-4.63**	-2.33	-1.94	-2.29	-2.43

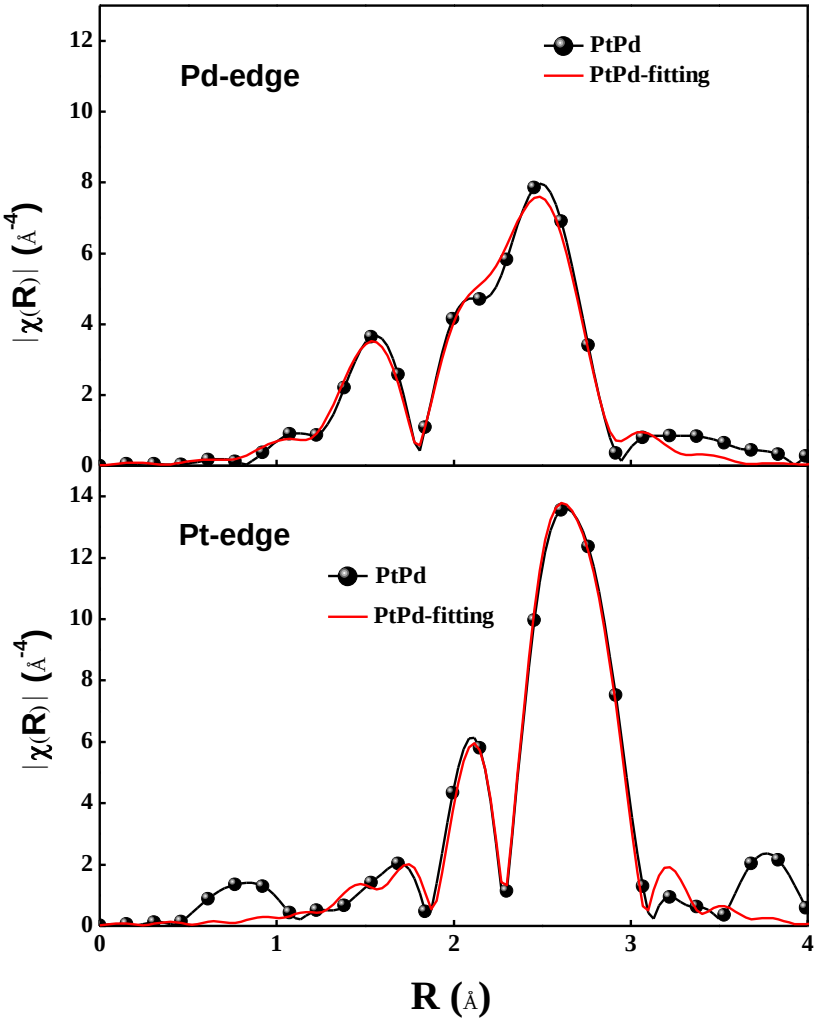

Figure S1 The EXAFS spectra of PtPd NRs.

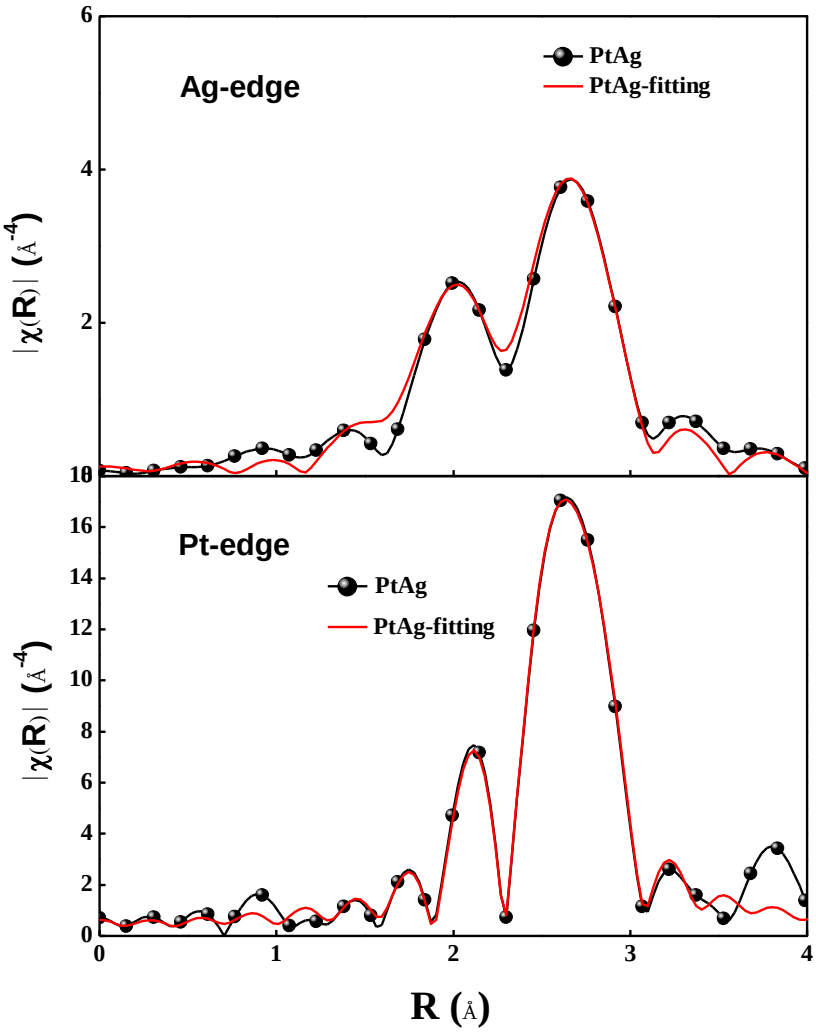

Figure S2 The EXAFS spectra of PtAg NRs.

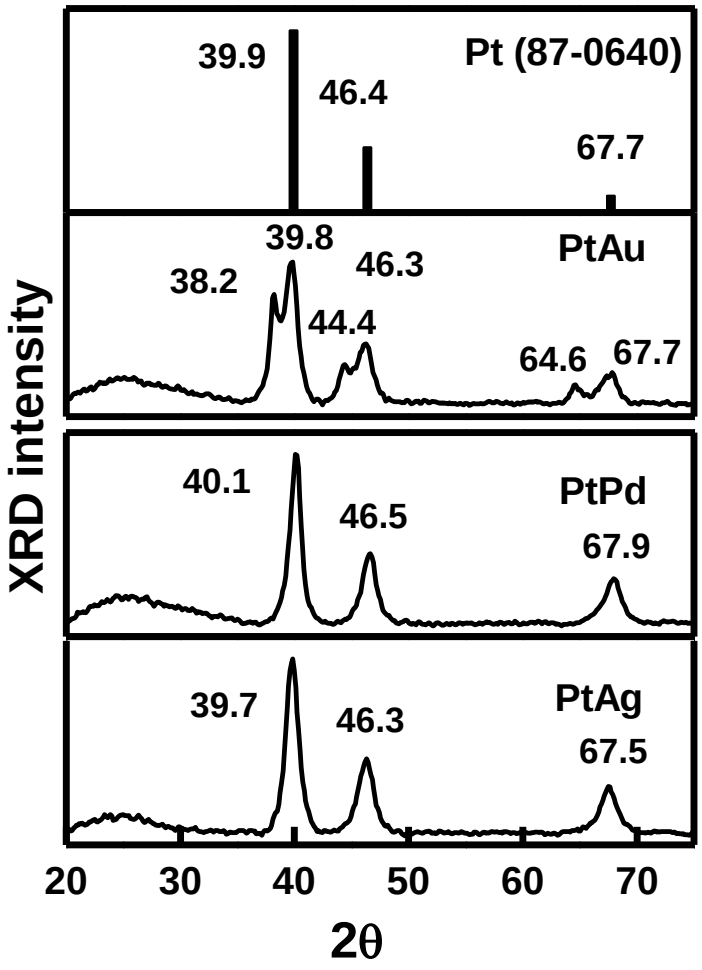

Figure S3 XRD patterns of PtM NRs.

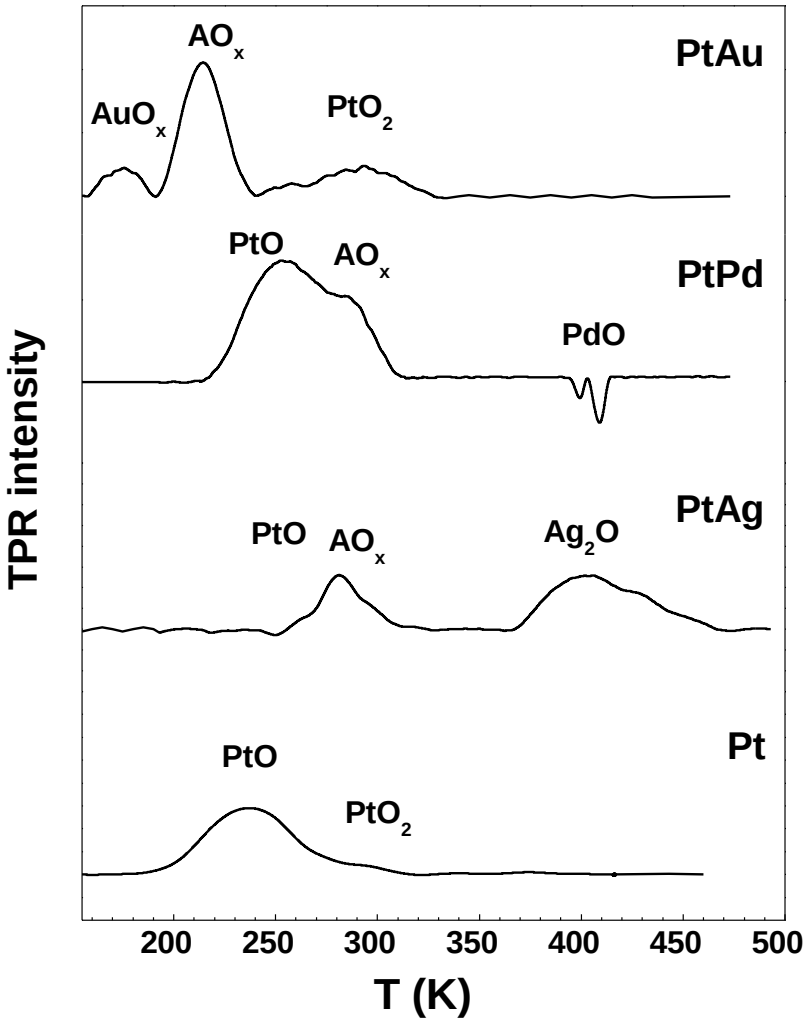

Figure S4 TPR analyses of PtM NRs after oxidation at 300 K.

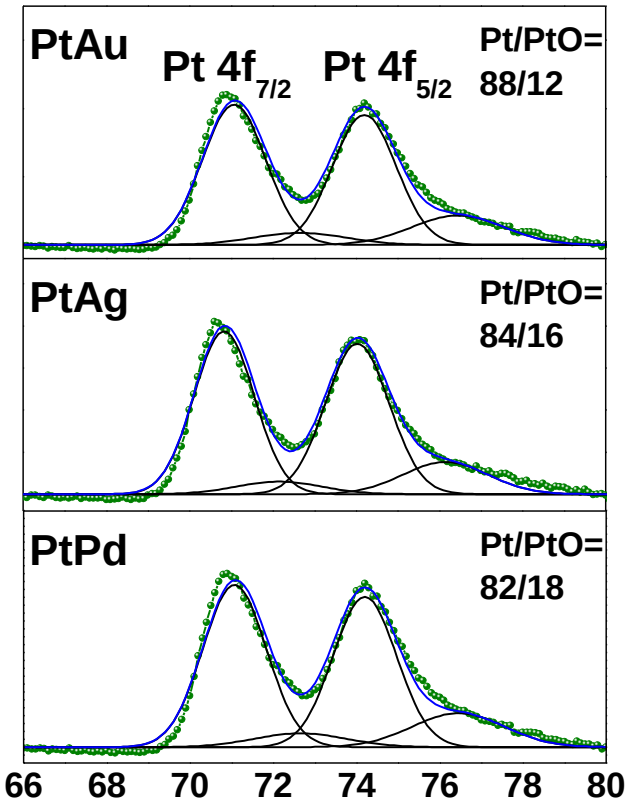

Figure S5 XPS spectra of Pt and fitting results for PtPd, PtAg, and PtAu NRs.

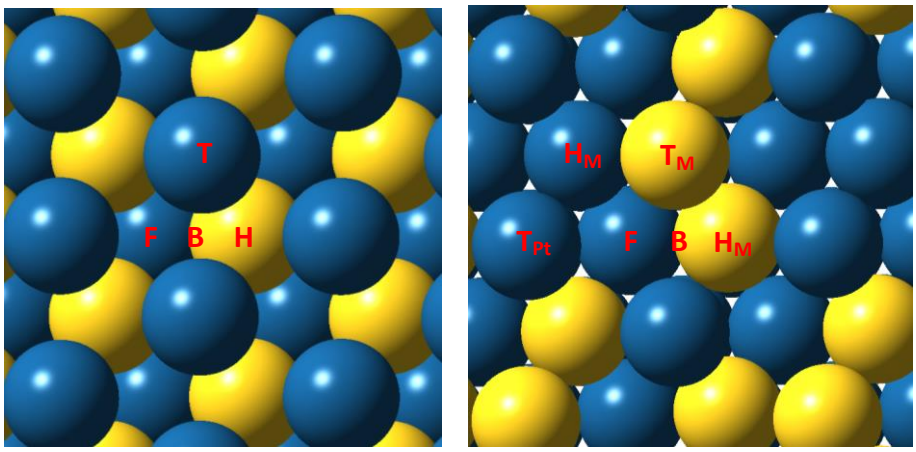

Figure S6 Adsorption sites on the modeled M@Pt (left) and Pt@M (right). T, B, H and F are top, bridge, hcp and fcc sites, respectively. The subscripts label the adsorptions on Pt and M atoms. Cyan and yellow spheres represent Pt and M atoms, respectively.

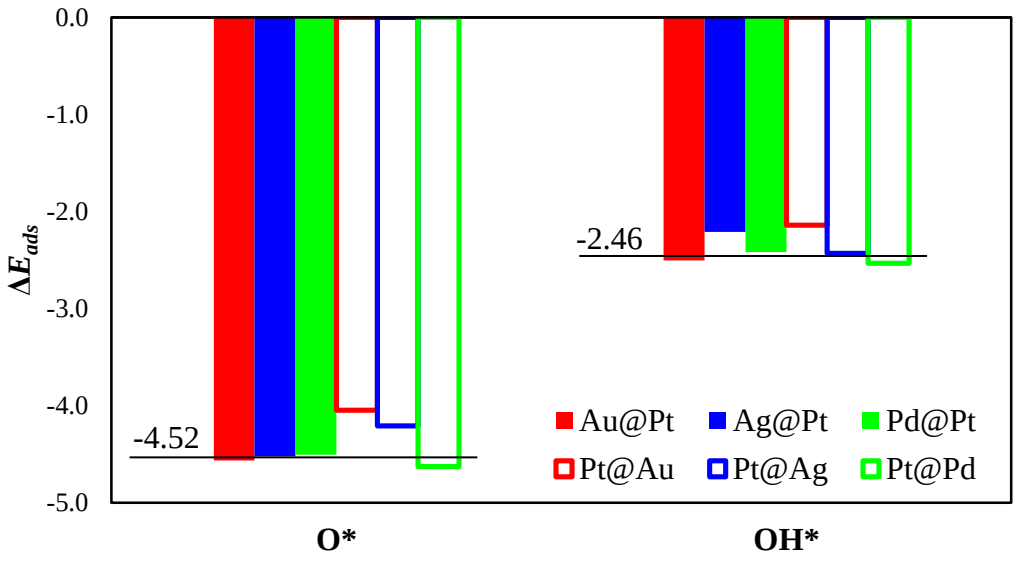

Figure S7 The E_{ads}(O*) and E_{ads}(OH*) on M@Pt (M core/Pt surface, solid bars), Pt@M (Pt core/M surface, open bars), and pure Pt surface (lines and numbers).

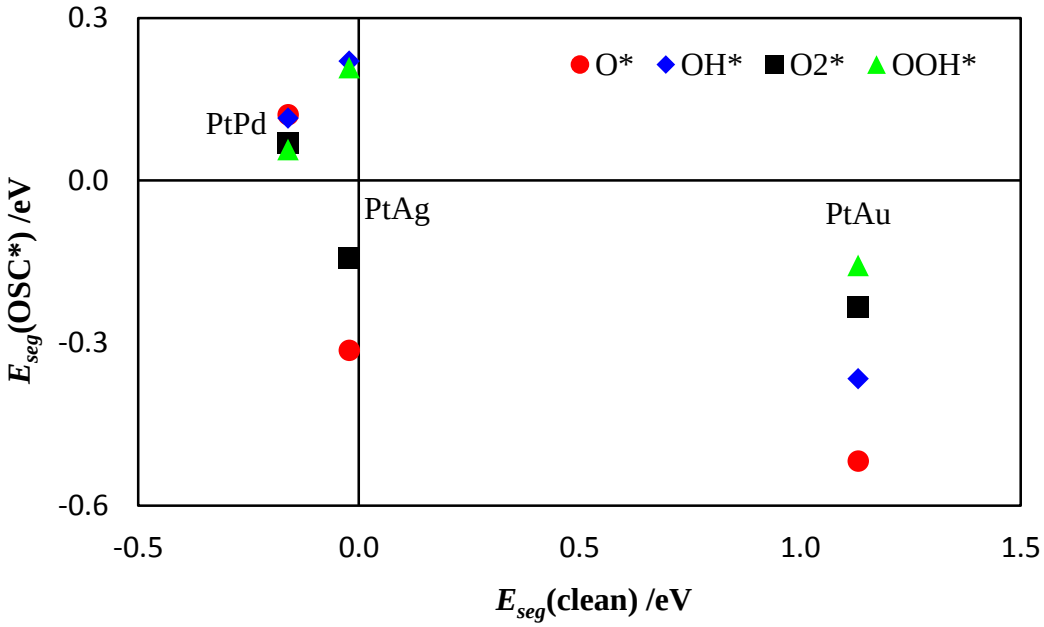

Figure S8 E_{seg}(clean) and E_{seg}(OCS*) for PtPd, PtAg and PtAu surfaces.